Journal of Thermal Analysis and Calorimetry, Vol. 72 (2003) 329–335

THERMAL ANALYSIS OF TWO Fe–X–B (*X*=Nb, ZrNi) ALLOYS PREPARED BY MECHANICAL ALLOYING

J. J. Suñol[*]*, A. González and J. Saurina*

GRMT, Dept. de Física, Universitat de Girona, Santaló s/n, 17071 Girona, Spain

Abstract

The alloys, $Fe_{60}Ni_{14}Zr_6B_{20}$ and $Fe_{85}Nb_9B_6$, were produced by mechanical alloying. The formation of the nanocrystallites (about 40 nm) was detected by X-ray diffraction. Furthermore, a slight oxygen presence (<3 at.%) was found by induced-coupled plasma and EDX microanalysis. After milling, calorimetry scans show low temperature recovery process and several crystallization processes related with the crystal growth and reordering of the crystalline phases. The apparent activation energies, 360 and 290 kJ mol^{-1}, were determined by the Kissinger method. A mass increase (about 1 mass%) was detected by thermogravimetry.

Keywords: crystallization, Fe–Zr and Fe–Nb based alloys, mechanical alloying

Introduction

Mechanical alloying (MA) represents a nonexpensive versatile route able to produce equilibrium as well as non-equilibrium materials including amorphous, nanostructured, composites, and extended solid solution systems [1–4]. In mechanical alloying, powder particles acquire energy of successive collisions and are subjected to a continuous disintegration with fragmentation as a result of the impact forces. The resulting fresh surfaces help reaggregation of the powdered components with the formation of new particles, where the elements become stacked in layers, then allowing diffusion of one into the others.

Amorphous Fe–Zr–B and Fe–Nb–B alloys containing α-Fe nanocrystallites with the bcc structure are of interest as a superior soft magnetic materials [5–7]. Usually, these alloys have been obtained by controlled crystallization of melt-spun amorphous ribbon precursors [8–12]. Furthermore, mechanical alloying is an alternative route to obtain directly the nanocrystals embedded in a residual amorphous phase [13]. In this paper we describe the thermal behavior of two Fe–X–B (*X*=Nb, ZrNi) nanocrystalline alloys produced by MA.

* Author for correspondence: E-mail: joanjosep.sunyol@udg.es

1388–6150/2003/ $ 20.00
Akadémiai Kiadó, Budapest

Experimental procedure

Mechanical alloying was carried out in a planetary high-energy ball mill (Fritsch Pulverisette P7) starting from pure element and compound powders (Fe of 99.7% purity, with a particle size under 10 μm; Nb of 99.85% purity, with a particle size under 74 μm; B of 99.6% purity, with a particle size 50 μm and Ni_7Zr_3 of 99% purity, with a particle size under 100 μm). The compositions analyzed in this article were $Fe_{85}Nb_9B_6$ and $Fe_{60}Ni_{14}Zr_6B_{20}$, labeled as A and B respectively. Each of the powder samples was loaded into a cylindrical Cr–Ni stainless-steel vial together with balls of the same material in an argon atmosphere. The balls to powder ratio was 5:1. The milling process was performed at a speed of 600 rpm for 10, 20, 40 and 80 h.

The sample thermal characterization was carried out by differential scanning calorimetry (DSC) under an argon atmosphere in a DSC30 equipment of Mettler-Toledo and by thermogravimetry (TG) in a TGA851 Mettler-Toledo equipment. The morphology and composition study was performed by scanning electron microscopy (SEM) in a DSM960 A Zeiss equipment with energy dispersive X-ray microanalysis (EDX) and by induced coupled plasma (ICP) in a Liberty-RL ICP Varian equipment. Complementary structural analysis of the milled powders by Mössbauer spectroscopy and X-ray diffraction is under study.

Results and discussion

The formation of the nanocrystalline structure during mechanical alloying was followed by X-ray diffraction. The nanocrystallites formed after 80 h milling were about 40 nm size [14]. The powder composition was followed by induced coupled plasma. The ICP results show slight (<3.0 at.%) contamination from the milling tools (Fe, Ni and Cr) and from the atmosphere (oxygen), similar results were found in Fe–Ni–P–Si mechanically alloyed powders [15]. Detected contamination increases with the milling time.

The morphology of the powders was followed by scanning electron microscopy. As an example Fig. 1 shows the micrographs that corresponds to alloy A after 20 (a) and 80 h (b) of milling. As increasing the milling time, the average grain size diminishes. EDX microanalysis of localized zones shows also the oxygen contamination due to the oxide formation.

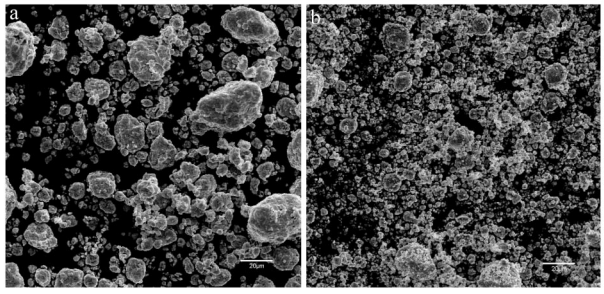

Fig. 1 SEM micrographs of alloy $Fe_{85}Nb_9B_6$ alloy after; a – 20 h MA and b – 80 h MA

Thermal study was performed by differential scanning calorimetry. Stability, an important factor on amorphous metallic structures is related to the relaxation phenomena and crystallization, which is usually a thermally activated process of transition from a disordered amorphous structure to an ordered crystal structure.

Figures 2 and 3 show DSC curves corresponding to alloys A and B respectively. After 10 h milling, all DSC scans show several reactions on heating. At low temperature, about 400 K, an exothermal process. This is a signature of recovery of stress, that is, mainly deformation energy stored during the milling process. Since it occurs in a wide temperature range it is often overlapped with exothermic peaks characteristic of structural transformations, such as reordering or crystallization/recrystallization processes. The late processes have generally well defined activation energy. On the contrary, recovery may be modeled by use of a wide spectrum of activation energies of the relaxation time [16]. As increasing the temperature, one or two crystallization processes appears related with the crystal growth and reordering of the crystal-

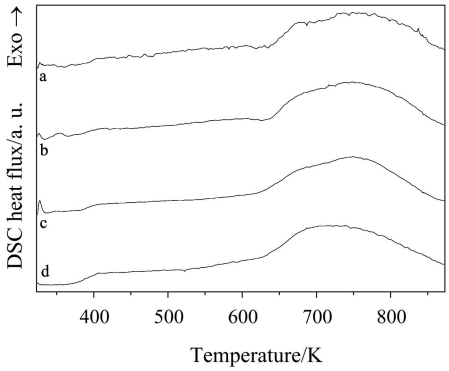

Fig. 2 DSC scans of alloy A ($Fe_{85}Nb_9B_6$) at a heating rate of 10 K min^{-1}; a – 10 h MA; b – 20 h MA; c – 40 h MA and d – 80 h MA

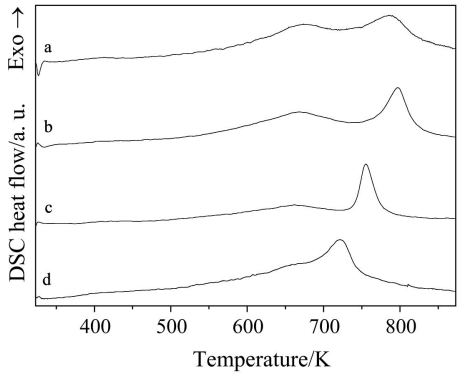

Fig. 3 DSC scans of alloy B ($Fe_{60}Ni_{14}Zr_6B_{20}$) at a heating rate of 10 K min^{-1}; a – 10 h MA; b – 20 h MA; c – 40 h MA and d – 80 h MA

line phases. Furthermore, the thermal stability and the crystallization kinetics were analyzed as a function of the milling conditions and alloy composition. As increasing the milling time, the thermal processes are the same and only slight changes in temperature and the increase of enthalpy associated to an increase of the amorphous phase content were detected.

The shape of the DSC scans of alloy A milled for 10 to 80 h are similar. At all times, the main crystallization processes began at about 625 K. Nevertheless, the enthalpy area associated to the crystallization increases in a factor 3. Furthermore, as increasing the milling time the recovery, associated to the wide process beginning at about 390 K, becomes more energetic.

The shape of the DSC scans of alloy B milled for 10 to 80 h are most differentiated. In all DSC two main crystallization peaks appear but the temperature interval of both process changes with the milling time. Moreover, the enthalpy area associated to the exothermic process increase only a 20%. After 20 h MA, as increasing the milling time decreases the thermal stability of the main crystallization peak.

The approach activation energy, E, for the main crystallization process of alloys milled 80 h can be evaluated using the Kissinger equation: $\ln(\beta/T_p^2)$ *vs.* $1/T_p$ with β the heating rate and T_p the peak temperature [17]. The crystallization data have been collected from DSC curves, obtained with different heating rates (2.5, 5, 10, 20 and 40 K min^{-1}). As an example, Fig. 4 shows the DSC scans of alloy B. The values obtained are 360±40 and 290±30 kJ mol^{-1} for alloy A and B respectively. Energy values of 320, 370 and 351 kJ mol^{-1} were found for $Fe_{87}Zr_7B_6$, $Fe_{86}Zr_7B_6Cu_1$ [18] and $Fe_{85.5}Zr_4Nb_4B_{5.5}Al_1$ [19]. All these values seem reasonable to be associated with a grain growth process. Obviously, the method used to obtain the activation energy influences the results. As an example, using the Ozawa method [20], the values obtained are 375±43 and 305±32 kJ mol^{-1} for alloy A and B respectively. Furthermore, in complex systems, if the activation energy depends on the degree of conversion, its values obtained by isoconversional and peak based methods are different [21]. Nev-

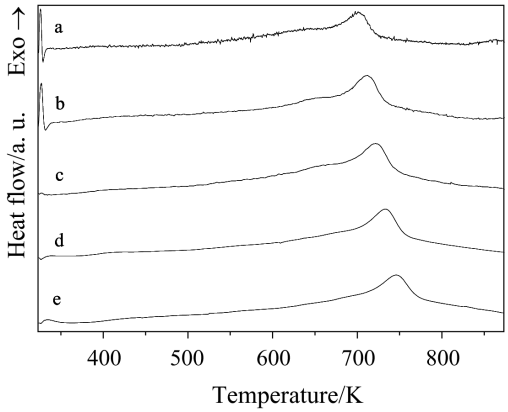

Fig. 4 DSC scans of alloy B ($Fe_{60}Ni_{14}Zr_6B_{20}$) at different heating rates under Ar atmosphere; a – 2.5 K min^{-1}; b – 5 K min^{-1}; c – 10 K min^{-1}; d – 20 K min^{-1} and e – 40 K min^{-1}

ertheless, the overlapping between structural relaxation and crystallization process difficult the use of isoconversional methods in our case and the comparative activation energies given in previous references were calculated using peak based analysis.

In the alloy A, the main crystallization peak is related to the crystalline growth of the α-Fe phase as detected by X-ray diffraction. The temperature broad process detected by DSC corresponds to different Fe environments. The two overlapped peaks present in the alloy B crystallization were also found in previous works [22–23] in Fe–Ni based alloys and are related to more complex crystallization. We can compare these results with the crystallization behavior of melt-spun ribbons for similar compositions reported in the bibliography [19, 24]. The as-quenched amorphous phase crystallizes in a two-stage crystallization process in which a single bcc α-Fe nanocrystalline phase appears after the first stage, and coarse α-Fe grains with intermetallic phases appears after the second stage [19]. This behavior was also found in Fe–M–B (*M*=Zr, Hf or Nb) alloys [24]. In all these alloys, to detect the second stage is necessary to use other equipment as a DTA to show the high temperature (>900 K) crystallization. Furthermore, the structural relaxation phenomenon of the mechanically tensioned powders is not so important in as-quenched ribbons [25]. The crystallization process of the as-quenched ribbons began at higher temperature. Therefore, the metastable phases obtained by rapid solidification are more thermally stable than analogous phases in mechanically alloyed powders [12, 25–26]. Similar behavior was found in nanocrystalline mechanically alloyed Fe–Zr–B–(Cu) alloys [27–28]. Moreover, new mechanically alloyed compositions are under study to analyze precursor influence in the MA process and in the thermal stability of the alloys.

Careful analysis of the crystallization and related process is needed. From TG scans of the milled powders in an inert atmosphere we detect an oxidation process that begins with the recovery as shown in Fig. 5, that corresponds to an FeZrNiB alloy. A small mass increase beginning at 400 K. Mass evolution may be explained by adsorption of residual oxygen present in the argon. Similar behavior was found in the thermogravimetry analysis of nanocrystalline Fe–Ni solid solutions prepared by me-

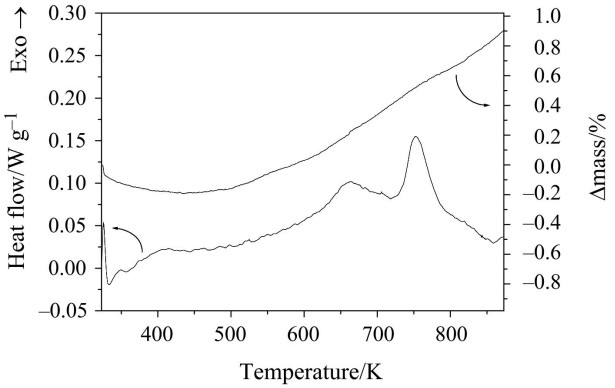

Fig. 5 Alloy FeZrNiB. DSC and TG scans at a heating rate of 10 K min^{-1} under argon atmosphere

chanical alloying [29]. The thermally induced structural changes produce a slight oxidation of the material.

Conclusions

Two Fe–X–B (*X*=Nb, ZrNi) alloys were produced in a nanocrystalline form by mechanical alloying. After 10 h milling, all DSC scans show several exothermic reactions on heating. At low temperature, beginning at about 400 K, a recovery process is found. As increasing the temperature, several crystallization processes appear related with the crystal growth and reordering of the crystalline phases. As increasing the milling time only slight changes in temperature and the increase of enthalpy was found in the alloy with Nb. As increasing the milling time decreases the thermal stability of the main crystallization process of ZrNi alloy.

The apparent activation energy, *E*, values for the main crystallization process of alloys A and B were 360±40 and 290±30 kJ mol^{-1} respectively. These values seem reasonable to be associated with a grain growth process. A slight oxide formation was found by microanalysis and by ICP. Furthermore, a thermally induced oxidation was detected by thermogravimetry.

* * *

Financial support from MICYT (project No. MAT2000-0388) and DURSI (project 2001SGR-00190) is acknowledged.

References

1 T. Nasu, K. Nagaoka, N. Itoh and K. Suzuki, J. Non-Cryst. Solids, 122 (1990) 216.
2 E. Hellstern and L. Schultz, Mater. Sci. Eng., 97 (1988) 39.
3 O. Kohmoto, N. Yamaguchy and T. Mori, J. Mater. Sci., 29 (1994) 3221.
4 K. A. Krivoroutchko, T. Kulik, V. I. Fadeeva and V. K. Portnoy, J. Alloys and Compounds, 333 (2002) 225.
5 K. Suzuki, N. Kataoka, A. Inoue, A. Makino and T. Masumoto, Mater. Trans. JIM., 31 (1990) 743.
6 J. van Wonterghem, S. Morup, C. J. W. Koch, S. W. Charles and S. Wells, Nature, 322 (1986) 622.
7 J. Shen, Z. Li, Q. Yan and Y. Che, J. Phys. Chem., 97 (1993) 8504.
8 Y. Yoshizawa, S. Oguma and K. Yamaguchi, J. Appl. Phys., 64 (1988) 6044.
9 G. Herzer, Mater. Sci. Eng. A, 133 (1991) 1.
10 K. Suzuki and J. M. Cadogan, J. Appl. Phys., 87–9 (2000) 7097.
11 P. Garcia-Tello, J. González, J. M. Blanco and R. Valenzuela, J. Appl. Phys., 87–9 (2000) 7112.
12 Y. Umakoshi, T. Nakano, T. Tsujimoto and W. Fujitani, Scripta Mater., 43 (2000) 349.
13 M. E. McHenry, M. A. Willard and D. E. Laughlin, Progr. Mat. Sci., 44 (1999) 291.
14 J. J. Suñol, A. González, J. Saurina, Ll. Escoda, T. Pradell, M. T. Clavaguera-Mora and N. Clavaguera, Rapidly Quenched & Metastable Materials Congress, Oxford 2002.

15 J. J. Suñol, Ll. Escoda, J. Saurina and J. Caleya. XXVIII Reunión Bienal de la RSEF, Sevilla 2001, p. 324.
16 M. T. Clavaguera-Mora, J. J. Suñol and N. Clavaguera, J. Metast. Nanocryst. Mater., 10 (2001) 459.
17 H. Kissinger, Anal. Chem., 29 (1957) 1702.
18 P. Duhaj, I. Matko, P. Svec, J. Sitek and D. Janickovic, Mater. Sci. Eng. B, 39 (1996) 208.
19 A.-H. Mansour and J. Barry, J. Mater. Sci. Letters, 17 (1998) 1127.
20 T. Ozawa, Bull. Chem. Soc. Jpn., 38 (1965) 1881.
21 P. Budrugeac, D. Homentcovschi and E. Segal, J. Therm. Anal. Cal., 63 (2001) 457.
22 J. J. Suñol, N. Clavaguera and M. T. Clavaguera-Mora, J. Non-Cryst. Solids, 287 (2001) 114.
23 J. J. Suñol, T. Pradell, N. Clavaguera and M. T. Clavaguera-Mora, J. Metast. Nanocryst. Mater., 10 (2001) 525.
24 A. Makino, K. Suzuki, A. Inoue and T. Masumoto. Mater. Sci. Eng. A, 179 (1994) 127.
25 T. Pradell, J. J. Suñol, N. Clavagueraa and M. T. Clavaguera-Mora, J. Non-Cryst. Solids, 276 (2000) 113.
26 Z. Caamaño, G. Pérez, L. E. Zamora, S. Suriñach, J. S. Muñoz and M. B. Baró, J. Non-Cryst. Solids, 287 (2001) 15.
27 M. Multigner, A. Hernando, P. Crespo, C. Stiller, J. Eckert and L. Schultz, J. Magn. Magn. Mater., 197 (1999) 214.
28 C. Stiller, J. Eckert, S. Roth, R. Schafer, U. Klement and L. Schultz, J. Non-Cryst. Solids, 207 (1996) 620.
29 V. Hays, R. Marchand, G. Saindrenan and E. Gaffet, Nanostruct. Mater., 7–4 (1996) 411.